First SMOS Sea Surface Salinity dedicated products over the Baltic Sea

Verónica González-Gambau[1], Estrella Olmedo[1], Antonio Turiel[1], Cristina González-Haro[1],
Aina García-Espriu[1], Justino Martínez[1], Pekka Alenius[2], Laura Tuomi[2], Rafael Catany[3], Manuel Arias[3],
Carolina Gabarró[1], Nina Hoareau[1], Marta Umbert[1], Roberto Sabia[4], and Diego Fernández[4]

[1]Barcelona Expert Center (BEC) and Institute of Marine Sciences (ICM), CSIC, P. Marítim de la Barceloneta, 37-49, 08003 Barcelona, Spain
[2]Finnish Meteorological Institute, Erik Palménin aukio 1, FI-00560 Helsinki, Finland
[3]ARGANS Ltd, Davy Road, Plymouth Science Park, Derriford, Plymouth, PL6 8BX, United Kingdom
[4]European Space Agency, ESA-ESRIN. Largo Galileo Galilei 1 Casella Postale 64 00044, Frascati, Italy

Correspondence: Verónica González-Gambau (vgonzalez@icm.csic.es)

Abstract.

This paper presents the first Soil Moisture and Ocean Salinity (SMOS) Sea Surface Salinity (SSS) dedicated products over the Baltic Sea. The SSS retrieval from L-band brightness temperature (TB) measurements over this basin is really challenging due to important technical issues, such as the land-sea and ice-sea contamination, the high contamination by Radio-Frequency

5 Interferences (RFI) sources, the low sensitivity of L-band TB at SSS changes in cold waters and the poor characterization of dielectric constant models for the low SSS and SST ranges in the basin. For these reasons, exploratory research in the algorithms used from the level 0 up to level 4 has been required to develop these dedicated products. This work has been performed in the framework of the European Space Agency regional initiative Baltic+ Salinity Dynamics.

Two Baltic+ SSS products have been generated for the period 2011-2019 and are freely distributed: the Level 3 (L3) product

10 (daily generated 9-day maps in a $0.25°$ grid, https://doi.org/10.20350/digitalCSIC/13859) (González-Gambau et al., 2021a) and the Level 4 (L4) product (daily maps in a $0.05°$ grid, https://doi.org/10.20350/digitalCSIC/13860) (González-Gambau et al., 2021b)), that are computed by applying multifractal fusion to L3 SSS with Sea Surface Temperature (SST) maps. The accuracy of L3 SSS products is typically around 0.7-0.8 psu. The L4 product has an improved spatio-temporal resolution with respect to the L3 and the accuracy is typically around 0.4 psu. Regions with the highest errors and limited coverage are located

15 in Arkona and Bornholm basins and Gulfs of Finland and Riga.

The impact assessment of Baltic+ SSS products has shown that they can help in the understanding of salinity dynamics in the basin. They complement the temporally and spatially very sparse in situ measurements, covering data gaps in the region and they can also be useful for the validation of numerical models, particularly in areas where in situ data are very sparse.

1 Introduction

20 The Baltic Sea is a strongly stratified semi-enclosed sea with a large freshwater supply from rivers, net precipitation and water exchange and high-saline water from the North Sea through the Danish Straits. The water exchange in the Danish Straits is

hampered by bathymetric (narrow and shallow sills) and hydrodynamic restrictions (fronts and mixing). The depth of the Baltic Sea is very shallow (54 m in average), which yields to highly variable ocean dynamics mainly controlled by local atmospheric forcing (Leppäranta and Myrberg, 2009). The bottom water in the sub-basins is mainly ventilated by major Baltic saltwater

25   inflows (Matthäus and Franck, 1992; Fischer and Matthäus, 1996).

Complex oceanographic conditions within the Baltic Sea are a challenge for oceanographic models and, for example, the salinity dynamics cannot be comprehensively simulated by the present model systems (e.g. Meier et al., 2006; Hordoir et al., 2019; Lehmann et al., 2021). Furthermore, model simulations of the Baltic Sea are constrained by the measurements available for calibrating and validating the models and compiling and assimilating the initial fields. Hence, additional satellite data is

30   crucial to improve the performance of the Baltic Sea models.

In-situ temperature and salinity observations in the Baltic Sea have been performed from research vessels since 1898. Traditionally, the countries around the Baltic Sea delivered data to International Council for the Exploration of the Sea (ICES). The present internationally coordinated monitoring data is collected under programs of HELCOM (http://www.helcom.fi), which is the governing body (1979, Helsinki) in the Convention on the Protection of the Marine Environment of the Baltic Sea.

35   There are other oceanography data portals that also include Baltic Sea data (e.g. SHARK, SeaDatanet, EMODnet, Baltic Nest Institute). The contents of these data sources are largely overlapping and, in general, the sampling of the in situ data is very heterogeneous in space and time.

Remote sensing has been used for decades in the Baltic Sea to follow the ice conditions, surface temperature and algal blooms. However, salinity conditions have remained outside of an overall synoptic view so far.

40   For all the above, Earth Observation sea surface salinity (SSS) measurements have a great potential to help in the understanding of the dynamics in the basin (Omstedt et al., 2014): they can complement temporally and spatially the in situ measurements in the region, and they also can be useful for validating numerical models, especially in those areas where in situ data are sparse. Nonetheless, the Baltic Sea is one of the most challenging regions for the SSS retrieval from L-band satellite measurements. The available EO-based global SSS products over this region are quite limited, both in terms of spatio-temporal

45   coverage and quality due to several technical limitations. In the case of SMOS (Soil Moisture and Ocean Salinity), there are two major sources of error strongly affecting the brightness temperatures (TB) measurements: (i) the high contamination by Radio-Frequency Interferences (RFI) sources (Oliva et al., 2016) and (ii) the contamination close to land and ice edges (Martín-Neira et al., 2016). The latter is particularly crucial in the TBs over the Baltic Sea: few points are further than 110 km from the nearest coast and the Bothnian Bay and the eastern part of the Gulf of Finland have ice cover every year and in severe winters

50   there is ice also in the Baltic Proper. Besides, since the sensitivity of L-band TB to SSS changes is very low in cold waters (Yueh et al., 2001), much larger errors than in temperate oceans are expected in the Baltic Sea, where the typical average values of the Sea Surface Temperature (SST) during winter are below the $3°C$. Moreover, available dielectric constant models were derived from salinity measurements in the range of the global ocean (32-38 psu) and they are not fully tested in the low SSS (typical average value of 7 psu) and low SST ranges of this basin. For all these conditioning factors, essential modifications

55   have been required in the algorithms from the very low level of processing up to the SSS retrieval methodology to develop dedicated SSS products over the Baltic Sea.

To improve the quality of the SMOS brightness temperatures, the technique focused on the correction of the correlators efficiency errors proposed by Corbella et al. (2015) is used to mitigate the land-sea and ice-sea contaminations. In the SSS retrieval, the two major changes with respect to the original Debiased non-Bayesian retrieval (Olmedo et al., 2017) used in the generation of the current global Barcelona Expert Center (BEC) SSS product (Olmedo et al., 2021b) are: (i) the empirical correction of the dielectric constant model for the low SST and low SSS regimes of the Baltic Sea, and, (ii) the characterization and correction of residual systematic errors of SSS, depending not only on the acquisition conditions, but also on the SST.

In this work, we present the dedicated algorithms used to develop the Baltic+ L3 and L4 SSS products and their quality assessment. The article is structured as follows: Section 2 describes the datasets (section 2.1) and algorithms (section 2.2) used in the generation of the Baltic+ SSS products. Section 3 presents the quality assessment of the SSS products. Section 3.1 presents the different datasets used for comparison and validation, section 3.2 describes the methods, section 3.3 explains the quality metrics used in the validation and section 3.4 shows the validation results. The conclusions are summarized in Section 4.

2 Generation of Baltic+ SSS products

2.1 Data sets used in the generation of the products

2.1.1 SMOS Brightness Temperatures

We generate the TB dataset starting from the SMOS ESA Level 0 data (https://smos-diss.eo.esa.int/oads/access/. Level 0 is the raw data containing both observation data and housekeeping telemetry.

2.1.2 Auxiliary data used in the salinity retrieval

The auxiliary data used for the SSS retrieval comes from the European Centre for Medium range Weather Forecast (ECMWF) (Sabater and De Rosnay, 2010). They can be accessed at https://smos-diss.eo.esa.int/oads/access/collection/AUX_Dynamic_ Open. ESA provides an ECMWF auxiliary file spatially and temporally colocated with each SMOS overpass. The following fields are used in the SSS retrieval: sea ice cover, rain rate, 10-meter wind speed, 10-meter neutral equivalent wind (zonal and meridional components), Significant Wave Height (SWH) of wind waves, 2-meter air temperature, surface pressure, and vertically integrated total water vapour (Zine et al., 2008).

We use a regional climatology as annual reference SSS field, which is added to the debiased SMOS SSS anomalies (see section 2.2.4). This regional climatology is distributed by SeaDataNet and provides temperature and salinity monthly climatologies computed from an historical dataset (mainly from CTD and discrete water samplers in the period 1900-2012) (SeaDataNet Baltic Climatology), with a spatial resolution of $0.11°$ in longitude and $0.065°$ in latitude. The salinity field at 0 m depth is used. Monthly climatologies are averaged to obtain an annual reference field. A nearest neighbor interpolation is used to compute the reference value at the grid of the debiased SMOS SSS anomalies.

2.1.3 Sea Surface Temperature

Since the SST is one important driver of the SSS errors, we analysed the errors of all the available SST datasets over the Baltic sea (ECMWF (Sabater and De Rosnay, 2010), OSTIA (Donlon et al., 2012), CMC (Canada Meteorological Center, 2012),

90 REMSS (Remote Sensing Systems, 2017), CCI (Merchant et al., 2019) and CMEMS Baltic Sea reanalysis (Axell, 2019)) by computing the differences with respect to the SeaDataNet in situ measurements (see section 3.1.3). We use the SST product that provided the best performance: the ESA Sea Surface Temperature Climate Change Initiative (SST CCI) Level 4 Analysis Climate Data Record, version 2.1 ((Merchant et al., 2019), https://data.ceda.ac.uk/neodc/esacci/sst/data/CDR_v2/Analysis/L4/ v2.1 for the period 2011-2016 and the Operational Sea Surface Temperature and Sea Ice Analysis (OSTIA) product for the

95 period 2017-2019 ((Donlon et al., 2012)).

The ESA CCI SST combines data from both the Advanced Very High Resolution Radiometer (AVHRR) and Along Track Scanning Radiometer (ATSR) SST_CCI Climate Data Records, providing daily global SST on a 0.05 degree regular latitude-longitude grid.

The OSTIA dataset uses satellite data provided by international agencies via the Group for High Resolution SST (GHRSST).

100 These products include data from microwave and infrared satellite instruments. The OSTIA dataset has also daily global coverage on a 0.05 degree regular latitude-longitude grid.

These SST products are used in the SSS retrieval (section 2.2.4), in the correction of SMOS SSS systematic biases (section 2.2.4) and as a template in the fusion scheme to generate the L4 SSS product (section 2.2.8).

2.1.4 Sea Ice Concentration

105 A sea-ice mask is required to discard those SSS retrievals in ice-covered regions. This sea-ice mask is created from the sea ice fraction (SIF) information provided by OSTIA (product ID "OSTIA-UKMO-L4-GLOB-v2.0", (Donlon et al., 2012)). We generate an ice filtering flag (SSS are discarded when SIF>0) in order to discard those raw SSS retrievals acquired when sea ice is present.

2.1.5 CMEMS Baltic Sea reanalysis

110 We use the Baltic Sea physics reanalysis (CMEMS_product_ID: BALTICSEA_REANALYSIS_PHY_003_011, (Axell, 2019)) for the temporal correction of the Baltic+ L3 SSS maps (see section 2.2.7) and for the estimation of the L4 SSS uncertainty (see section 2.2.9). This product provides a 24 years (1993-2019) reanalysis for the Baltic Sea using the ice-ocean model NEMO-Nordic and the LSEIK data assimilation scheme. Daily mean salinity at 1.5 m depth (the uppermost available salinity) are used to generate 9-day salinity fields at $0.25°$ with the same temporal coverage than the SMOS L3 SSS maps.

2.1.6 Three-dimensional coupled sea ice-ocean model of the Baltic Sea (BSIOM)

We use the daily SSS of the BSIOM hindcast simulation using the model configuration described in (Lehmann et al., 2014) with ERA5 atmospheric forcing. The horizontal resolution of the coupled sea-ice ocean model is 2.5 km, and we use the uppermost salinity of the 60 vertical levels. This data is used for the estimation of the L4 SSS uncertainty (see section 2.2.9).

2.2 Algorithm description

2.2.1 Generation of brightness temperatures

Some of the corrections we propose to improve the quality of TBs over the Baltic Sea are not included in the current operational ESA L1B products. For this reason, we have used the MIRAS Testing Software (MTS) (Corbella et al., 2008), developed by the Universitat Politècnica de Catalunya (UPC), that provides TBs at antenna reference frame from SMOS ESA level 0 data, to generate the TB dataset.

We use the ALL-LICEF mode as the calibration approach (Corbella et al., 2016). The main advantage of using this calibration mode is that the measurements of the zero-baseline visibility, and the rest of the visibility samples, are more consistent. The up-to-date methods developed by the UPC in the recent years for reducing image reconstruction errors are also included in the MTS. Details on the used image reconstruction strategy can be found in Corbella et al. (2009, 2019).

2.2.2 Mitigation of errors in SMOS brightness temperatures

Corbella et al. (2015) showed that the dominant contribution to both Land/Sea Contamination (LSC) and the Ice/Sea Contamination (ISC) comes from residual multiplicative errors and proposed a 2% correction factor to the MIRAS correlator efficiencies (also known as the G_{kj} correction).

The application of this correction leads to an overall reduction of the TB contamination close to the coasts (Corbella et al., 2015). This enhancement is also reflected globally in the quality of the SSS retrievals from the corrected TBs (González-Gambau et al., 2017).

In the Baltic, the ALL-LICEF calibration approach and the G_{kj} correction are crucial to reduce the LSC/ISC close to coasts and ice edges. As an indicator of the TB quality, the differences between the SMOS TB measurements and the theoretically modeled TBs at ocean surface (hereafter referred to TB anomaly) are analyzed. Details on the derivation of the modeled TBs can be found in González-Gambau et al. (2017).

The impact of the G_{kj} correction on the SMOS TB over the Baltic Sea is shown in Figure 1. A significant overall reduction of the systematic biases is observed in the whole basin ($\sim 2 - 3$ K), improving the quality of TBs.

González-Gambau et al. (2015); González-Gambau et al. (2016) proposed a dedicated technique, the Nodal Sampling (NS), to mitigate the impact of RFI contamination. This technique has been successfully applied at a global scale (González-Gambau et al., 2017) and in the Black Sea (Olmedo et al., 2021a). However, the application of the NS for the specific case of the Baltic
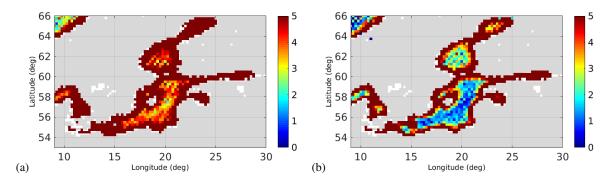
Figure 1. 9-day $0.25°$ map (June 2014) of the mean anomaly ($TB_{SMOS} - TB_{mod}$) of the First Stokes parameter divided by two [K]. (a) TB without the G_{kj} correction, (b) TB after applying the G_{kj} correction.

145 Sea did not show a significant improvement, indeed this is the unique basin where we did not find it. Further investigation is required to fully understand the reasons of this under-performance.

Before the salinity retrieval process, the corrected brightness temperatures are transformed from antenna to ocean surface as detailed in section 2.2.2 of Olmedo et al. (2021a).

2.2.3 Empirical correction of the dielectric constant model for the Baltic Sea

150 The SSS retrieval is based on finding the appropriate value of raw SSS that makes the GMF of TB closer to the actually measured TB. The GMF is derived from a dielectric constant model for sea water. All the dielectric constant models found in the literature are built by empirical fitting of laboratory measurements. The dielectric constant model of Klein and Swift (Klein and Swift, 1977) has been used until recently in the operational SMOS L2OS (Level 2 Ocean Salinity) processor. The dielectric constant model of Meissner and Wentz (M&W) (Meissner and Wentz, 2004; Meissner et al., 2018) is used in Aquarius and 155 SMAP salinity processors. The M&W model was reported as more suitable at low SST ranges (Meissner and Wentz, 2004; Zhou et al., 2017). Therefore, we propose to use the M&W dielectric constant model to retrieve SSS in the Baltic Sea.

In a first analysis of the retrieved raw SSS, a low number of retrievals was obtained in some regions of the Baltic, specially in regions where the SSS values are very low. Figure 2 (a) shows the difference between the SMOS and the modelled TB (i.e., the TB associated to the retrieved raw SSS using the GMF) for all the measurements in 2013 under the following acquisition con-160 ditions (latitude, longitude, overpass direction, across-track distance, incidence angle): ($\varphi = 56, \lambda = 19, A, x = 0, \theta = 42.5$). Those values for which a salinity retrieval is obtained are marked with green circles.

It was found that raw SSS values were only retrieved if $TB_{meas} - TB_{mod} \leq 0$. In the Baltic Sea, the values of SSS and SST are very low and the sensitivity of SSS to TB is also very low at cold waters. Thus, large biases on TB translate to large biases on SSS, what typically leads to negative raw SSS values in the retrieval. These negative salinity values do not have any 165 physical meaning; they just reflect the presence of instrumental biases that must be corrected.

The M&W dielectric constant model is reviewed for the SST and SSS conditions of the Baltic Sea. Figure 2 (b) shows the modelled half first Stokes parameter as a function of the salinity for a given incidence angle ($40°$) and SST ($0°C$). The
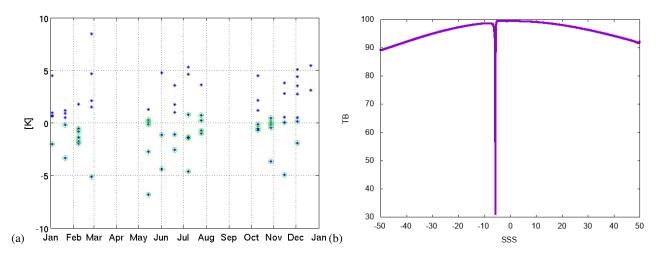
Figure 2. (a) Difference of SMOS and modeled TB (blue stars) for ascending orbits in 2013 for the following acquisition conditions: (φ=56,λ=19,A,x=0,θ=42.5). Green circles indicate those measurements for which a valid SSS is retrieved. (b) Half First Stokes modeled TB (MW model) versus raw SSS for $\theta = 40°$ and $T_s = 0°C$.

problems at low SSS values are evident: the dielectric model presents at least a maximum value for very low SSS, what causes an inversion problem for TB values that are close to this maximum (i.e., the same TB can be attributed to two different SSS values). This behaviour of the models is non-physical and come from the fact that models are constructed by polynomial fitting of experimental observations taken at the typical salinity values for the global ocean, (i.e, in the range of [32-38] psu) and, therefore, the value of the dielectric constant at low SSS is an extrapolation.

For very diluted solutions, the conductivity depends almost linearly on the salinity, as shown in Figure 3. For low concentrations of salt ions (low enough to neglect interactions among ions), conductivity and emissivity depend on the amount of available ions. Thus, for low SSS, the dielectric constant should also depend almost linearly with salinity.

However, as shown in Figure 2 (b), MW model starts deviating considerably from the almost linear dependence on SSS at about 20 psu. Therefore, lacking of a better characterization of the dielectric constant at low SSS, we decided to perform a linear extension of M&W dielectric constant model for SSS lower than 20 psu.

2.2.4 Debiased non-Bayesian SSS retrieval

The debiased non-Bayesian (DNB) SSS retrieval (Olmedo et al., 2017) focuses on the correction of the residual systematic biases in SSS (produced by LSC and permanent RFI) and on the increase of coverage with respect to the standard (Bayesian) retrieval algorithm. The original debiased non-Bayesian approach has been fine-tuned for retrieving SSS in the Baltic Sea. Major modifications are highlighted in this section.

Non-Bayesian salinity retrieval

A single SSS value is retrieved for each TB measurement (at a given incidence angle), unlike the conventional Bayesian retrieval, where a single SSS is retrieved from the entire set of multi-angular TB. Details on the retrieval of SSS (referred as
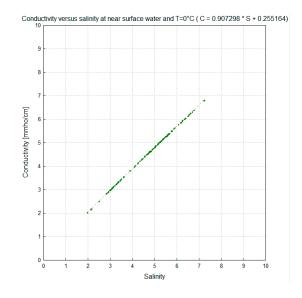
Figure 3. Conductivity versus SSS for $SST = 0°$. An almost linear relationship exists between conductivity and salinity.

raw SSS) can be found in section 2.2 of Olmedo et al. (2017).These raw SSS are then appropriately classified, filtered, and combined, to build global SSS maps.

Definition of a SMOS-based climatology

190   We want to characterize the systematic errors in SMOS SSS. This characterization is based on the hypothesis that systematic errors are the same for all those SSS acquired under the same conditions. Seven years of SMOS SSS retrievals (2013-2019, the cleanest period in terms of RFI contamination) are used for the characterization of those systematic biases on raw SSS that do not depend on time.

   The raw SSS are grouped together according to their geolocation in the same fixed grid of TB measurements (coordinated by
195   the latitude (φ) and longitude (λ)), overpass direction (ascending or descending, denoted by d), across-distance to the center of the swath (in 50-km bins, denoted by x) and incidence angle (in $5°$ bins, denoted by θ). Then, for each group, we use the central estimator for characterizing the systematic biases of this group. We call this central estimator the SMOS-based climatology (see the original DNB method in Olmedo et al. (2017) for more details).

   When we applied the original DNB retrieval to the Baltic Sea, we observed that seasonal variations were much higher than
200   in the global ocean (Olmedo et al., 2020) and a non-expected spatial gradient appeared close to the coasts. These effects were evidenced when computing the monthly mean difference between SMOS SSS and CMEMS Baltic reanalysis salinity field (Figure 4).

   Then, we analyzed the dependence of these differences on SST. SMOS SSS fields retrieved in 2013 were collocated with the salinity and temperature outputs from the CMEMS Baltic reanalysis. Figure 5 shows the mean of the difference between
205   the salinity, as observed by SMOS, and the reanalysis for each bin of $1°C$ of SST. To mitigate these systematic spatial biases
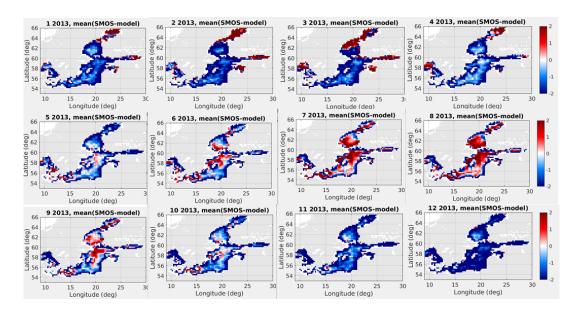
Figure 4. Maps of monthly mean differences between SMOS SSS and the salinity field of CMEMS Baltic reanalysis.

dependent on SST, we modify the original DNB to include the SST (T_s) as one more parameter in the classification of the SSS retrievals for the computation of the SMOS-based climatology.
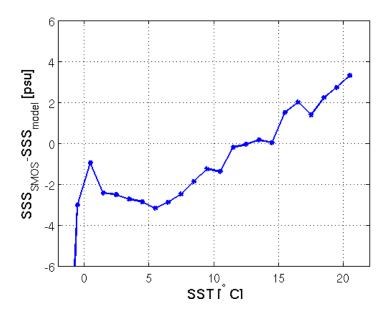

Figure 5. Difference between the SMOS SSS and reanalysis salinity variability as a function of the SST.

Therefore, for each given 6-tuple (instead of the 5-tuple of the original DNB), $c = (\varphi, \lambda, d, x, \theta, T_s)$, all the raw SSS retrievals $SSS(\varphi, \lambda, d, x, \theta, T_s)$ in the period 2013-2019 are accumulated. To avoid lack of statistics, seven bins of SST (note that bin

210 size varies depending on the SST range) are defined with a certain overlap for the low ranges of SST (see Table 1).

Bin	SST [$^\circ C$]	Range of SST to be applied [$^\circ C$]
1	< 4	< 2
2	< 6	$[2, 4]$
3	$[2, 8]$	$[4, 6]$
4	$[4, 10]$	$[6, 8]$
5	$[6, 12]$	$[8, 10]$
6	$[10, 15]$	$[10, 15]$
7	> 15	> 15

Table 1. Bins of SST and the corresponding ranges of SST to be applied.

The classification of the raw SSS for the 6-tuple leads to SMOS-based climatological distributions with a significantly reduced number of events. For this reason, the strategy for computing the SMOS-based climatology, i.e., the central estimator of all the raw SSS acquired under a given 6-tuple, is changed with respect to the original DNB. We base the computation only on the first and second order moments. In the Baltic Sea, the presence of outliers in the raw SSS highly impacts on

215 the estimation of the statistical parameters that characterize the SMOS-based climatological distributions. To avoid this, the statistics are computed only with raw SSS belonging to the interval between the 5-quantile (IQ5) and the 95-quantile (IQ95). Hence, the mean (m_0) and the standard deviation (σ_0) of the distributions are computed in the interval [IQ5,IQ95]. Then, the SMOS-based climatology (denoted as sss_{clim}) is defined for a given acquisition condition as the averaged value of the raw SSS in the interval $[m_0 - \sigma_0, m_0 + \sigma_0]$.

220 **Generation of debiased non-Bayesian SMOS salinities**

For the generation of the debiased non-Bayesian SMOS SSS values, each raw SSS acquired at a time t and at the given acquisition condition $(\varphi, \lambda, d, x, \theta, T_s)$ is corrected with the corresponding SMOS-based climatology sss_{clim}, thus giving the SMOS-based anomalies.

Then, a time-independent SSS reference is added to the SMOS SSS anomalies to obtain the final debiased SSS values. The

225 annual reference SSS field used is the Baltic regional climatology provided by SeaDataNet (see section 2.1.2).

We study now whether the multi-annual mean of the salinity (required for the bias mitigation) changes with SST. To assess it, the impact of adding the regional SSS climatology computed per bins of SST versus using a unique regional climatology as the annual reference field is analyzed. We use the SSS and SST provided by CMEMS Baltic reanalysis in the period 2013-2019 to compute the averaged SSS for each bin of SST. The mean error when using the single regional climatology as the annual

230 reference field, instead of using the mean SSS value per bin of SST (taking into account the frequency of each SST value), is

shown in Figure 6. The typical error is around 0.05 psu, except in the Danish straits, where can reach up to 0.4 psu. Since this error is, in general, quite low in the basin, a single annual reference field is used to generate the debiased SMOS SSS.
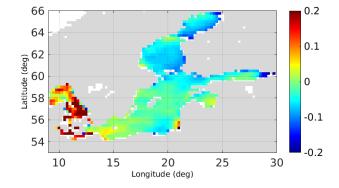

Figure 6. Mean error when applying a single annual reference climatology instead of a different climatology computed per each bin of SST.

2.2.5 Filtering criteria

Errors in SSS retrievals over the Baltic Sea are expected to be much larger than in the global ocean, due to the low sensitivity of
235 SSS to TB at cold waters. Moreover, residual errors caused by land/sea and ice/sea contamination, as well as perturbations by RFI sources, are also affecting the salinity retrievals. For this reason, the filtering criteria defined for the BEC global product (Olmedo et al., 2021b) are not suitable for this basin. In this work, the filtering criteria are reviewed to be less restrictive while giving accurate enough values for the Baltic Sea.

The filtering criteria are the following:

240 - Any raw SSS out of the range [-150, 100] psu is not considered as part of the valid raw SSS values.

- For a given 6-tuple, $c = (\varphi, \lambda, d, x, \theta, T_s)$, the SMOS-based climatological distribution under at least one of these conditions is discarded:

  - The histogram has less than 30 measurements.

  - The standard deviation is greater than 35 psu.

245 If the SMOS-based climatological distribution corresponding to a given 6-tuple has been discarded following the previous criteria, then all the associated raw SSS are discarded.

- Raw SSS are discarded if they are considered too much deviated from the SMOS-based climatology. Therefore, any raw SSS value outside the interval defined by $[m_0 - \sigma_0, m_0 + \sigma_0]$ (see section 2.2.4) is discarded.

- In order to improve the quality of L3 SSS maps, all SSS values with an associated uncertainty (estimated as detailed in
250 section 2.2.2 of Olmedo et al. (2021b)) larger than 2 psu are also discarded before the generation of the L3 map. These

11

points mainly correspond to ice-covered areas during the cold season, such as the Bothnian Bay and the Gulf of Finland, as well as some grid points closest to the coast.

- After applying the temporal correction (section 2.2.7), the SSS values outside the range [0, 35] psu are also discarded. SSS retrievals in the Skagerrak and the Kattegat straits (grid points with longitudes lower than $14°E$) are also filtered out because of the large SSS uncertainties in the region, mainly during the cold season (see section 2.2.6).

2.2.6 Generation of SSS for a given satellite overpass and L3 maps

The Baltic+ L3 SSS data product is provided in a regular longitude-latitude grid of $0.25°$ (final grid). All the debiased and filtered SSS obtained for a given grid point in one overpass are averaged using an area-weighted average. An extrapolated value of SSS can be assigned to the cells of the final grid, by conveniently weighting the contributed values for each overlapping cell of the original grid (Lambert Azimuthal Equal Area grid of 25 km). We compute the L3 SSS maps by weight-averaging the SSS of the different overpasses in a 9-day period. Each contributing SSS is weighted by the inverse of its error variance.
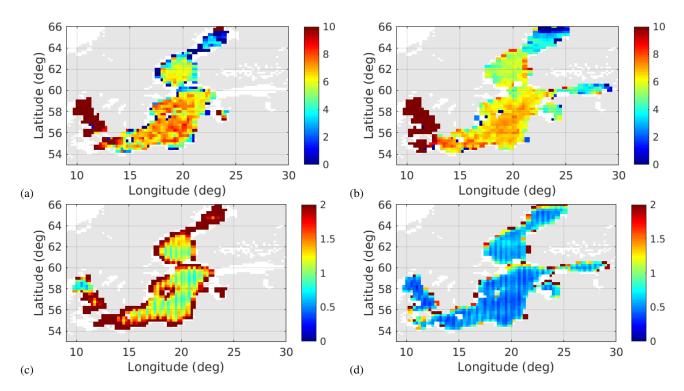

Figure 7. (a) 9-day $0.25°$ L3 SSS map 15th to 23rd January 2013, (b) 9-day $0.25°$ L3 SSS map 15th to 23rd July 2013, (c) Error of SSS map in (a), (d) Error of SSS map in (b).

An example of a L3 SSS map and its associated error are shown in Figure 7 for the cold (November to May) and warm (June to October) seasons. The estimated SSS error in the L3 product comes from the propagation of the errors in the debiased non-Bayesian SSS (in essence, coming from radiometric errors on TB). Note the increase of uncertainty in the winter period

265 (7(c)) with respect to summer period (7(d)). These larger errors in the cold season are expected due to the loss of TB sensitivity to SSS changes at cold waters.

2.2.7 Mitigation of time-dependent biases

SMOS measurements are affected not only by spatial biases, but also by biases that depend on time (Martín-Neira et al., 2016). In the debiased non-Bayesian retrieval, time-dependent biases are not corrected: the SMOS-based climatologies integrate a

270 multi-year period, providing a reference that is constant in time (section 2.2.4). Therefore, an additional correction for the time-dependent biases is required.

In the BEC global product (Olmedo et al., 2021b), the assumption used to mitigate these time-dependent biases is that the spatial average of SSS anomalies in the global ocean is zero at any instant. This hypothesis has been shown to hold well with in situ SSS (Argo) in the global ocean. But this assumption is not suitable regionally, and even more in the Baltic Sea due to the

275 net exchanges of salinity across region boundaries. In other BEC regional SSS products, such as the ones of the Mediterranean Sea (Olmedo et al., 2018b) and the Arctic Ocean (Olmedo et al., 2018a), time-dependent biases were corrected by using Argo measurements as reference. However, due to the lack of Argo floats, this approach cannot be applied in the Baltic Sea. Instead, we assess the temporal correction by using two different reference datasets: in situ measurements from SeaDataNet (section 3.1.3) and the CMEMS Baltic reanalysis (section 2.1.2). As it can be observed in Figure 8, both corrections are in agreement.

280 However, due to the lack of in situ measurements and their spatio-temporal inhomogeneity, the temporal correction computed with in situ is much noisier and not always provides a value for the correction, what leads to data gaps. For these reasons, the CMEMS Baltic reanalysis is used for the temporal correction.
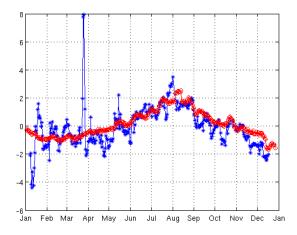

Figure 8. Temporal bias correction computed for the SSS product during 2013 by using the CMEMS Baltic reanalysis (red) and SDN in situ measurements (blue).

2.2.8 Multifractal fusion of SSS and SST

L4 SSS product has been generated by applying multifractal fusion techniques (Umbert et al., 2014; Olmedo et al., 2016),
285 which allows to reduce the noise of the SSS maps (Turiel et al., 2014) without loosing effective spatial resolution (Olmedo
et al., 2016). The application of this technique is aimed at improving the spatio-temporal resolutions of the Baltic+ L3 SSS
maps to approach user requirements (Baltic+ team, 2019).

The same SST data that is used as auxiliary data in the SSS retrieval, is used here as template in the fusion scheme. L4 SSS
maps are produced with the same spatio-temporal resolutions as the template, i.e., daily maps at a spatial grid of $0.05° \times 0.05°$.
290 Before applying the fusion, the salinity field from CMEMS Baltic reanalysis is used to complete the coverage where SMOS
L3 SSS is not available. Salinities from reanalysis are previously filtered by using the SIC information available in the SST
product. Figure 9 shows the number of times per year (as ratio to one) where the salinity reanalysis is used at each grid cell of
the L4 map. Overall, those regions with extrapolated values coming from the reanalysis are reduced to the gulfs, Bothnian Bay
and in those cell grids closest to coast. As it can be observed, during the first period of the mission (mainly during 2011-2012),
295 the reanalysis is also occasionally used in other regions when the maps are strongly affected by RFI contamination (Oliva
et al., 2016). For filtering purposes, a flag included in the product indicates if the SSS provided at each pixel comes from an
extrapolated reanalysis value.

2.2.9 Estimation of the L4 SSS error

To assess the inherent uncertainty of the L4 SSS product, the Correlated Triple Collocation (CTC) method is used (González-
300 Gambau et al., 2020). When applying CTC, the data are assumed to represent similar spatio-temporal scales and that two of
the datasets can have correlated errors. Under these conditions, CTC can be used to obtain maps of error variances of triplets
of remote sensing SSS maps.

We consider three sets of collocated SSS maps in the period 2016-2018: (i) Baltic+ L4 SSS product, (ii) CMEMS Baltic
reanalysis product (Axell, 2019) and (iii) the BSIOM hindcast simulation (section 2.1.6). As it is shown in Figure 7, the L3
305 SSS error during the cold season is higher than in the warmer season. Since the expected errors are quite different between
both seasons, we performed the CTC analysis for the warm and the cold seasons separately. This analysis is done with all
the products reduced to the common resolution (that of Baltic+ L4, 0.05 degrees and daily frequency). Figure 10 shows the
estimated error standard deviations of Baltic+ L4 SSS. L4 SSS errors are around 0.4-0.6 psu. These errors are in agreement to
the differences found in the comparison to in situ measurements (see validation section 3.4). There is a very significant error
310 reduction in the L4 SSS with respect to the L3 SSS (0.6-0.9 psu, see section 3.4.3). Note that, unlike the overall reduction of
the error in the warmer season for the L3 SSS product, in the case of the L4 SSS product there is not a clear improvement
for any of the seasons. This is likely due to the errors present in the SST employed as a template in the fusion scheme for the
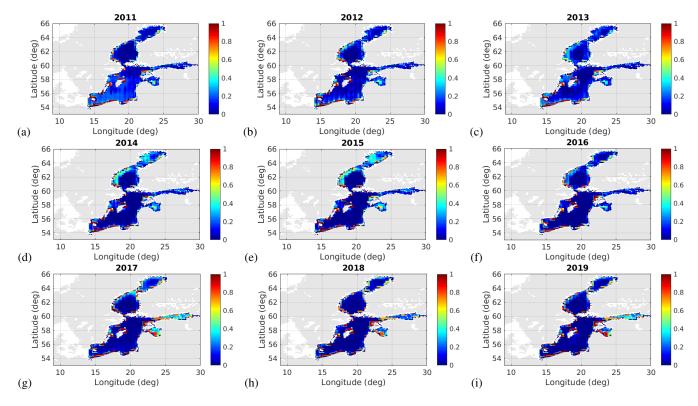generation of the L4 SSS product.

Figure 9. Ratio of time when the SSS from CMEMS Baltic reanalysis is used in those gridpoints where the SMOS SSS L3 product is not available (from (a) 2011 to (i) 2019).
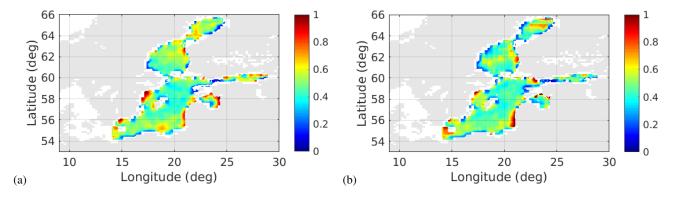

Figure 10. Error standard deviations computed by CTC for Baltic+ L4 SSS during (a) cold season, (b) warm season.

3 Quality assessment

3.1 Datasets for validation

3.1.1 Satellite Sea Surface Salinity

We compare the performance of the new Baltic+ SSS to those of other existing EO SSS products. The satellite SSS products used for this inter-comparison are the following:

- SMOS CATDS: 9-day SMOS SSS maps provided by Centre Aval de Traitement des Données SMOS (CATDS). We use the L3 debiased v5 freely available at: https://www.seanoe.org/data/00417/52804/#79565 (Boutin et al., 2018, 2020).

- ESA CCI: 7-day CCI SSS product. We use the v1.7 (Boutin et al., 2019).

- SMAP JPL: 8-day SMAP SSS maps are provided by Jet Propulsion Laboratory (JPL). We use the Level-3 version 4.2 freely available at https://podaac-opendap.jpl.nasa.gov/opendap/allData/smap/L3/JPL/V4.2/ (JPL Climate Oceans and Solid Earth group, 2019; Fore et al., 2016).

- SMAP REMSS: The 8-day running Remote Sensing Systems SMAP Level 3 Sea Surface Salinity Standard Mapped Image version v4 is used, which is freely available at http://www.remss.com/missions/smap. In particular, we have used the smoothed measurement at approximately 70 km resolution (Remote Sensing Systems (RSS), 2019; Meissner et al., 2018).

Figure 11 shows the spatio-temporal coverage during 2016 (percentage of valid SSS retrievals with respect to the total number of maps in the year) per each one of the above-mentioned satellite SSS products. The SMOS CATDS product shows very limited temporal and spatial coverage. SMAP JPL L3 SSS product exhibits a very good temporal and spatial coverage and SMAP REMSS covers mainly the central part of the basin with a good temporal coverage. The ESA CCI SSS product, developed from SMOS and SMAP measurements, shows a very limited spatial coverage but with good temporal coverage.

3.1.2 FerryBox lines in situ salinity

Ship tracks from the FerryBox voluntary network measure both temperature and salinity in mounted thermosalinographs (TSG) in voluntary vessels, making routinely transects in the Baltic Sea.

The data collected from these vessels pass quality control checks before being distributed to the science community. All the ship routes available for the validation of Baltic+ SSS products are collected in Table 2. They are used for validation depending on data availability (i.e. each ship track has different operating time) and its quality check passed as "good data" (PSAL_QC=1).
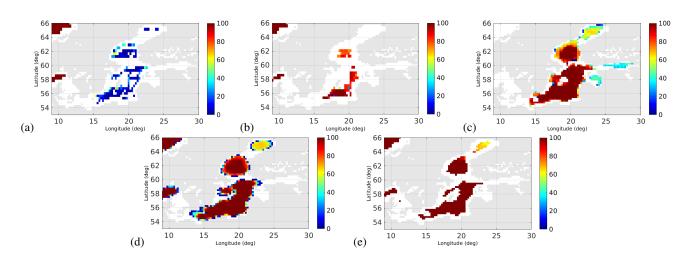
Figure 11. Spatio-temporal coverage of year 2016 (percentage of valid SSS retrievals with respect to the total number of maps in the year) per each satellite product: (a) SMOS CATDS, (b) ESA CCI, (c) Baltic+ L3 SSS, (d) SMAP JPL, (e) SMAP REMSS.

Ship route	Operating period	Spatial coverage
BalticQueen	2015-2018	Gulf of Finland
FinnMaid	2011-2018	South-North Baltic Proper to the Gulf of Finland
SiljaSerenade	2014-2018	Horizontal transect at $60°N$
Transpaper	2011-2018	Western coast of the Baltic, from the South to the Bothnian Sea
Victoria	2015-2016	Horizontal transect at $60°N$

Table 2. FerryBox ship routes and periods of operation.

3.1.3 SeaDataNet in situ salinity

SeaDataNet (SDN) Temperature and Salinity historical data collection for the Baltic Sea V2 (DOI 10.127701610aa44-0436-4b53-b220-98e10f17a2d4) contains all open access temperature and salinity in situ data retrieved from SeaDataNet infrastructure (CTD and discrete water samplers) until the end of 2014. Data has been quality checked using Ocean Data View software.

345 Quality flags of anomalous data have been revised using basic quality control procedures. For this validation, the following SSS and SST quality control provided within SDN dataset is applied: var3_qc=49 (good quality of SSS) and var2_qc=49 (good quality of SST).

The in situ data in the period 2015-2019 was downloaded from ICES (International Council for the Exploration of the Sea) Oceanography CTD and bottle data (nowadays ICES Data Portal https://www.ices.dk/). Data quality in ICES is solely on the

350 responsibility of the data originator, though ICES data center may do random quality checks for the data.

Furthermore, to keep consistency with the other datasets, the uppermost available SSS measurements are used for this validation, lying in the range of [1-5] m depth.

3.2 Validation methods

3.2.1 Collocation strategy of satellite-in situ data

355 The collocation strategy we follow for the comparison to in situ is the following:

- Spatial collocation

    - Ferrybox lines: These datasets provide SSS information at a very high temporal frequency. The location of in situ data are gridded to the nearest satellite grid cell, so, all the in situ measurements corresponding to the same cell grid in the satellite SSS product ($0.25°$ in the case of the L3 product and $0.05°$ in the L4 product) are averaged.

360   - SeaDataNet: In this dataset the temporal sampling is quite sparse. Several measurements in depth are available at each station. We consider that the water in the upper 5 meters is homogeneously mixed and it is representative of the surface water. Thus, we keep the shallowest measurement acquired between [1-5] meters depth, to be compared with the satellite SSS. The location of in situ data are referred to the nearest satellite grid cell and compared to the corresponding Baltic+SSS measurement. In this case, in contrast to the case of the Ferrybox measurements, almost

365   no average of in situ in a single grid is expected.

- Temporal collocation

    - For all the datasets, all the in situ available in the 9 days (for L3 product) of SMOS data used to generate the product, and in the same day (for L4 product) of the map are considered in the comparison.

3.3 Quality metrics for the comparison to in situ

370 The quality assessment of the SSS satellite retrievals results from the comparison against the reference datasets presented in sections 3.1.2 and 3.1.3. The validation metrics are based on statistical measurements of the difference between the two quantities at the collocations ($\Delta SSS = SSS_{sat} - SSS_{insitu}$).

The following metrics are computed both for Baltic+ L3 and L4 SSS products:

- Global statistics of ΔSSS for the datasets per year.

375 - Analysis of the products performances in the cold and warm seasons separately. The separation in these two periods is based in the expected SST ranges for the different months and the expected SSS error due to those SST values. The cold season ranges from November to May (average temperature of $3.9°C$) and the warm season refers to the period of June to October (average temperature of $13.4°C$). This analysis per seasons is devoted to assess if a quality improvement is observed during the warmer months, since the sensitivity increases and lower SSS errors than at colder temperatures are

380   expected.

18

- Maps of the spatial distributions of ΔSSS statistics: the temporal mean and the temporal standard deviation of ΔSSS are computed per each grid point in the map. This metric is devoted to track the possible origin of the errors (residual land sea contamination, sea-ice contamination, ice contamination itself, etc).

3.3.1 Correlated Triple Collocation

385 The three satellite SSS products with the finest temporal and spatial coverage (see section 3.1.1) are inter-compared. It must be pointed out that the salinity values provided by each one of the three satellite products are very different between them. We applied the CTC analysis using one year period (2016), which suffices to evaluate the performance of the datasets. Three sets of collocated SSS maps are considered: JPL SMAP v4.2 SSS, 8-day maps; REMSS SMAP v4.0 SSS, 8-day maps and Baltic+ L3 SSS, 9-day maps. We only consider Baltic+ L3 SSS here because it is the product with similar spatio-temporal resolutions as

390 JPL and REMSS SMAPS maps, a condition needed to apply the CTC method. In this triplet, the two variables with correlated errors are the JPL and REMSS products, both from SMAP measurements. Time collocation is done by identifying the first day of the three periods used in the generation of the corresponding maps. As JPL SMAP and REMSS SMAP maps are 1-day shorter, time collocation is not perfect but differences are considered to be negligible taking into account the orbital gaps in a 9-day period. Spatial collocation is straightforward, since the three products are provided in the same grid.

3.3.2 Baltic+ SSS variability and comparison to reanalysis and in situ data

395 The objective of this assessment is to analyse the SSS dynamics captured by Baltic+ SSS products and the CMEMS Baltic reanalysis (Axell, 2019) and to compare them to the 22 in situ observation stations visited by research vessels (Figure 12). Those stations are intended to cover different types of sea areas: from coastal regions to open sea. We choose the uppermost salinity observations, which means observations from 1 - 1.5 meters depth.

400 Time-series of Baltic+ L3 and L4 SSS products are analysed and compared to the salinity provided by the CMEMS Baltic reanalysis and the in situ measurements. For that, we define boxes over given regions of interest where, both, the reanalysis salinity and the Baltic+ L3 and L4 SSS products are averaged and compared to the in situ stations that are located in the region defined by each box. The boxes used for each region are shown in Figure 12.

3.4 Validation Results

3.4.1 Comparison to FerryBox lines salinity

405 All the in situ measurements from the different ferry routes are considered per year. The statistics are computed considering all the collocations available for the Baltic+ L3 SSS product and FerryBox data (see Table 3). Note that the number of match-ups corresponds to all the collocated measurements of SMOS and ferry data. The applied strategy is that, all the in situ measurements corresponding to the same cell grid of the satellite SSS product ($0.25°$ in the case of the L3 product), are

410 averaged. In overall, similar statistics are obtained for all the years. In the year 2012 there is a significant reduction of the
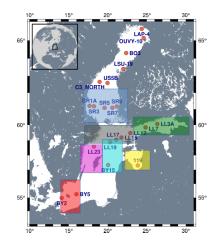
Figure 12. Map of the in situ stations and the boxes used in the analysis of the time-series per each region. Red: Arkona basin, grey: Northern Baltic Proper, blue: Bothnian Sea, cyan: Eastern Gotland basin, pink: Western Gotland basin, green: Gulf of Finland, yellow: Gulf of Riga.

accuracy due to the strong RFI affectation in the North Atlantic for that period (Oliva et al., 2016). Slightly higher biases are found for years 2014 and 2015.

Year	Mean	Median	STDD	R	Match-ups
2011	-0.16	-0.2	0.88	0.87	3827327
2012	0.21	0.16	1.12	0.73	6240087
2013	-0.19	-0.18	0.84	0.85	6835592
2014	-0.23	-0.23	0.86	0.83	10026054
2015	-0.21	-0.22	0.81	0.83	12565303
2016	-0.16	-0.17	0.83	0.87	7089550
2017	0.03	0.02	0.87	0.81	13384262
2018	-0.19	-0.16	0.85	0.88	8951692

Table 3. Global statistics Baltic+ L3 SSS product against FerryBox in situ data. Note the high variability in the number of match-ups is due to the different cruises operated each year. Per columns: year, mean, median, standard deviation (STDD), correlation coefficient (R) and number of collocations (Match-ups).

To analyse the spatial distribution of the differences (ΔSSS) between the Baltic+ L3 SSS product and the in situ provided by ferry lines, we compute the mean of ΔSSS (Figure 13), and the standard deviation of ΔSSS (Figure 14), for all the measurements accumulated during one year, for each cell of the Baltic+ L3 SSS product grid. The number of match-ups in the year per each grid cell is shown in Figure 15. Note that only grid cells with more than 10 accumulated measurements are considered. Higher standard deviation values are obtained for those cells closer to coast and ice edges, particularly close to

Gotland, in the Arkona and Bornholm basins, and in the Bothnian Bay. Errors in these regions notably increase the standard deviation when computing the statistics considering all the match-ups differences (see Table 3).

420   To analyze the spatial distribution without the effect of the non-homogeneous spatial sampling, the histograms of the spatial distributions of the mean and the standard deviation of ΔSSS are computed (not shown). The most probable value of the mean ΔSSS for the L3 product is in the range of [-0.35:-0.15] and the most probable value for the standard deviation of ΔSSS ranges between [0.57:0.72], depending on the year and it reaches 0.97 for the year 2012 (affected by strong RFI contamination).

Figure 13. Comparison of L3 SSS and ferry data: Spatial distribution of the mean of ΔSSS per year (from (a) 2011 to (h) 2018).

Global statistics are also computed considering all the collocations available for the Baltic+ L4 SSS product and FerryBox
425   data (see Table 4). We can observe a clear reduction of the standard deviation and an increase of the correlation coefficient with respect to the statistics computed for L3 SSS product (see Table 3). Similar biases to the ones for L3 product are found for the L4 product. This is expected because the fusion methodology aims at reducing the noise but not the biases present in the original L3 maps (Turiel et al., 2014).

We compute also global statistics of the collocations of Baltic+ L4 SSS and FerryBox data per year, considering only those
430   Baltic+ L4 SSS that come from the L3 SSS (i.e., extrapolated data from reanalysis are filtered out) (see Table 5). As it can be seen by comparing to the statistics considering all the measurements in the L4 product (Table 4), statistics have not significantly changed.
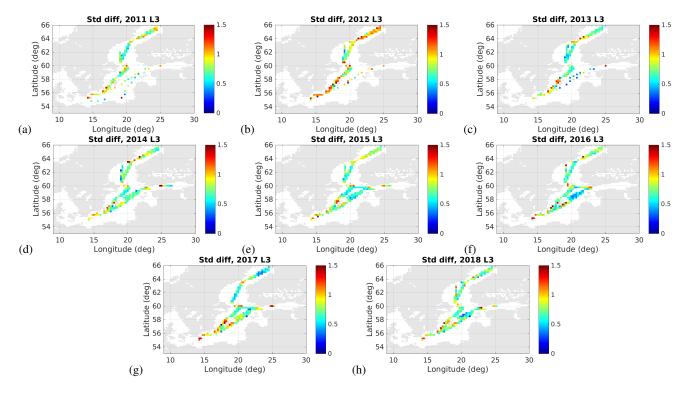
Earth System
Science
Data

Figure 14. Comparison of L3 SSS and ferry data: Spatial distribution of the standard deviation of ΔSSS per year (from (a) 2011 to (h) 2018).

Year	Mean	Median	STDD	R	Match-ups
2011	-0.11	-0.12	0.55	0.94	481038
2012	0.15	0.07	0.73	0.89	781871
2013	-0.15	-0.14	0.55	0.93	854449
2014	-0.2	-0.19	0.56	0.92	1254285
2015	-0.21	-0.25	0.57	0.91	1585228
2016	-0.08	-0.1	0.53	0.94	890838
2017	-0.05	-0.08	0.56	0.87	1678201
2018	-0.1	-0.08	0.52	0.92	1119688

Table 4. Global statistics Baltic+ L4 SSS product against ferrybox in situ data.

The spatial differences between the L4 SSS and the SSS provided by ferry data are computed in $0.05°$ grid of the L4 product (not shown). However, due to the low number of accumulated measurements for each grid cell, measurements are accumulated in a coarser grid ($0.25°$) to have significant statistics (see Figures 16, 17, 18). Besides, grid cells with accumulated
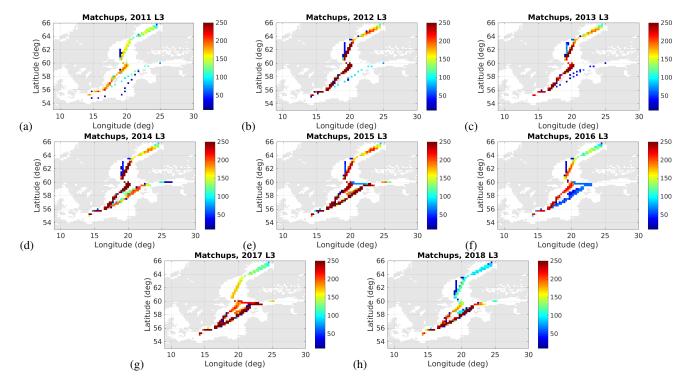
Figure 15. Comparison of L3 SSS and ferry data: Number of match-ups per each gridpoint in the map per year (from (a) 2011 to (h) 2018).

Year	Mean	Median	STDD	R	Match-ups
2011	-0.14	-0.17	0.57	0.94	362726
2012	0.2	0.13	0.76	0.87	594404
2013	-0.16	-0.17	0.58	0.93	633280
2014	-0.21	-0.21	0.58	0.9	933735
2015	-0.22	-0.25	0.58	0.9	1187949
2016	-0.1	-0.12	0.55	0.93	727614
2017	-0.04	-0.08	0.59	0.86	1143172
2018	-0.14	-0.12	0.54	0.91	773918

Table 5. Global statistics Baltic+ L4 SSS v2 product against FerryBox in situ data. L4 data has been filtered out to not consider extrapolated measurements from reanalysis (flag=1).

measurements lower than 10 are filtered out. The standard deviation is reduced in all the basin with respect to the L3 product (see Figure 17 in comparison to Figure 14). The histograms of the spatial distributions of the mean and the standard deviation

of ΔSSS are also computed. The most probable value of the mean ΔSSS for the L4 product is in the range of [-0.35:-0.25] psu and the most probable value for the standard deviation of ΔSSS ranges between [0.33:0.47] psu, depending on the year.
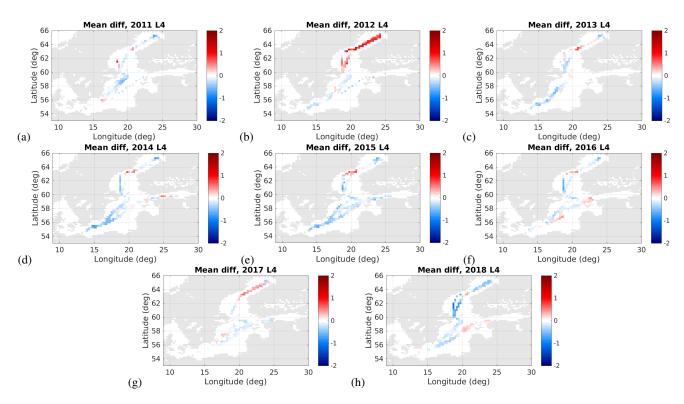

Figure 16. Comparison of L4 SSS and ferry data: Spatial distribution of mean ΔSSS per year (from (a) 2011 to (h) 2018).

3.4.2 Comparison to SeaDataNet salinity

Global statistics are computed considering all the collocations available for the Baltic+ L3 SSS product and SeaDataNet data per year (see Table 6). In overall, statistics are in agreement to the statistics of the comparison to the FerryBox data. However, higher values of standard deviation are obtained. This is likely due to the fact that Arkona and Bornholm basins are highly sampled with respect to the rest of the Baltic Sea and these regions present higher SSS errors.

The spatial distribution of the SeaDataNet in situ measurements allows us to analyse the performances of the Baltic+ L3 SSS product in the whole Baltic basin and the influence of the proximity to land and ice edges in the quality of the Baltic+ SSS products. We compute the mean of ΔSSS and the standard deviation of ΔSSS for all the measurements accumulated for each cell of the Baltic+ L3 SSS product grid. Measurements are accumulated in the original L3 grid ($0.25°$) for all the 9 years, since there are not enough in situ observations to perform the analysis per year separately, as we do in the case of FerryBox data. Since the number of match-ups is still quite limited, we compute the same maps by accumulating the measurements in a $0.5°$. In this way, we increase the number of measurements in each cell to get significant statistics. In addition, all those grid
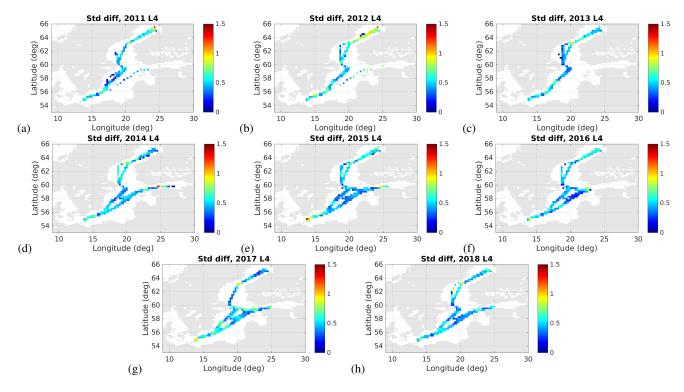
Figure 17. Comparison of L4 SSS and ferry data: Spatial distribution of the standard deviation of ΔSSS per year (from (a) 2011 to (h) 2018).

Year	Mean	Median	STDD	R	Match-ups
2011	-0.2	-0.19	1.06	0.73	4526
2012	-0.15	-0.09	1.36	0.46	8352
2013	-0.2	-0.21	0.94	0.68	9695
2014	-0.32	-0.31	0.97	0.7	5689
2015	-0.4	-0.36	0.95	0.6	11619
2016	-0.35	-0.37	1.05	0.74	7871
2017	-0.26	-0.3	1.03	0.73	7701
2018	-0.22	-0.19	0.91	0.73	10009
2019	-0.17	-0.12	1.06	0.75	8742

Table 6. Global statistics Baltic+ L3 SSS product against SeaDataNet in situ data. Per columns: year, mean, median, standard deviation (STDD), correlation coefficient (R) and number of collocations (Match-ups).

cells with less than 10 measurements are discarded. Higher errors are detected in Arkona and Bornholm basins, which are highly sampled regions. We also repeat this spatial analysis for the cold and the warm seasons. In the warm season the standard
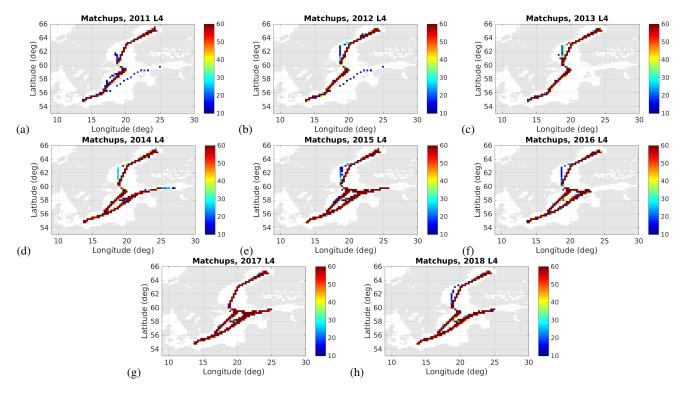
Figure 18. Comparison of L4 SSS and ferry data: Number of match-ups per each gridpoint in the map per year (from (a) 2011 to (h) 2018).

deviation is significantly reduced with respect to the cold season, as expected. The most probable value of the mean ΔSSS for
455 the L3 product is -0.15 in the cold season and -0.35 during the warm season. For the standard deviation of ΔSSS, the most
probable value is around 0.72 in the warm season and 0.78 in the cold season, although other mode appears around 1.05.

Figure 19. Spatial distribution of ΔSSS with SDN in a coarser grid (0.5°): (a) mean, (b) standard deviation, (c) number of match-ups.

Global statistics are computed considering all the collocations available for the Baltic+ L4 SSS product and SeaDataNet
data per year (see Table 7). Overall, statistics are in agreement to the statistics of the comparison to the ferry data. However,
higher values of standard deviation have been obtained. This is likely due to the fact that Arkona and Bornholm basins are
460 highly sampled with respect to the rest of the Baltic Sea basin and these regions present higher SSS errors. In any case, the

26

improvement in terms of the standard deviation and correlation coefficient with respect to the L3 SSS product is very significant
(see Table 6).

Global statistics are also computed considering all the collocations available for the Baltic+ L4 SSS product when the
extrapolation of the reanalysis data is not considered and SeaDataNet data per year (see Table 8). As it can be observed by
465 comparing to the statistics when considering all the measurements in the L4 product, statistics have not significantly changed
for most of the years. Higher differences are found for years 2011 and 2012, where the extrapolated data are not limited to the
coastal pixels (see Figure 9).

Year	Mean	Median	STDD	R	Match-ups
2011	-0.16	-0.09	0.63	0.87	917
2012	-0.15	-0.14	0.79	0.73	1459
2013	-0.16	-0.14	0.58	0.84	1603
2014	-0.25	-0.22	0.56	0.9	987
2015	-0.32	-0.31	0.59	0.83	1780
2016	-0.3	-0.31	0.71	0.88	1242
2017	-0.23	-0.25	0.61	0.87	1349
2018	-0.16	-0.16	0.58	0.89	1629
2019	-0.11	-0.1	0.73	0.87	1510

Table 7. Global statistics Baltic+ L4 SSS product against SeaDataNet in situ data. Per columns: year, mean, median, standard deviation
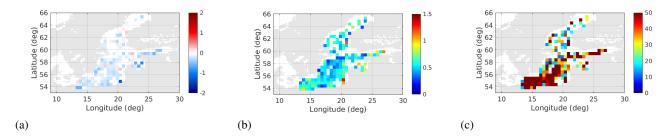(STDD), correlation coefficient (R) and number of collocations (Match-ups).

The spatial distribution of the differences between the Baltic+ L4 SSS product (considering all the measurements) and the in
situ provided by SeaDataNet is also analyzed. For that, we compute the mean of ΔSSS and the standard deviation of ΔSSS
470 for all the measurements accumulated in each cell of a $0.5°$ grid (to get significant statistics) (see Figure 20). Measurements
have been accumulated per all the 9 years since the match-ups are not enough to perform the analysis per year separately.
In agreement to the analysis of the L3 product, higher errors are detected in Arkona and Bornholm basins, which are highly
sampled regions. We perform this spatial analysis for the cold and the warm seasons separately. Once again, for the warm
season the standard deviation is reduced with respect to the cold season, as expected. The most probable value of the mean
475 ΔSSS for the L4 product is -0.25 in the cold season and -0.35 during the warm season. For the standard deviation of ΔSSS,
the most probable value is around 0.47 in the warm season while during the cold season is around 0.53.

3.4.3 Estimated SSS uncertainty by CTC

Maps of the estimated error standard deviations per each SSS dataset are shown in Figure 21. Notice that the estimated errors
for the Baltic+ L3 SSS are in agreement with the differences found with respect to in situ measurements (see sections 3.4.1
480 and 3.4.2). Differences between both SMAP products and the Baltic+ L3 SSS are shown in Figure 22. As shown in the figure,

Year	Mean	Median	STDD	R	Match-ups
2011	-0.2	-0.16	0.69	0.85	570
2012	-0.14	-0.14	0.86	0.66	1019
2013	-0.18	-0.22	0.61	0.82	1185
2014	-0.29	-0.28	0.59	0.88	692
2015	-0.33	-0.32	0.61	0.78	1418
2016	-0.32	-0.33	0.74	0.85	953
2017	-0.23	-0.28	0.59	0.87	938
2018	-0.18	-0.18	0.55	0.87	1200
2019	-0.09	-0.09	0.75	0.85	1078

Table 8. Global statistics Baltic+ L4 SSS product against SeaDataNet in situ data. L4 data is filtered out to not consider the extrapolated measurements from reanalysis. Per columns: year, mean, median, standard deviation (STDD), correlation coefficient (R) and number of collocations (Match-ups).

Figure 20. Comparison of L4 SSS and SDN: Spatial distribution of ΔSSS (0.5° grid): (a) mean, (b) standard deviation, (c) number of match-ups.

the Baltic+ L3 SSS product has the smallest error in the whole basin, except in some grid points of the Bothnian Bay, where the SMAP REMSS product presents a lower error.

Figure 21. Error standard deviations [psu] for the satellite SSS products computed by CTC for all the collocated maps in 2016: (a) SMAP-JPL (mean error in the basin: 2.81 psu), (b) SMAP-REMSS (mean error: 0.83 psu), (c) Baltic+ L3 SSS (mean error: 0.56 psu).
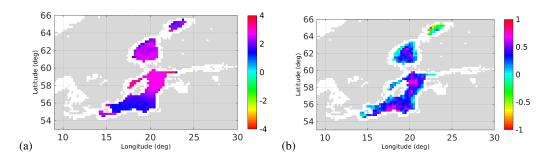
Figure 22. (a) Difference between SMAP JPL and Baltic+ L3 SSS error standard deviations [psu], (b) difference between SMAP REMSS and Baltic+ L3 SSS error standard deviations.

The analysis of the Baltic+ L3 SSS product and the comparison with the other satellite products reveals that the Baltic+ L3 SSS product is currently the satellite-derived SSS product with the lowest salinity error among the currently available products,
485 highlighting specially the improved spatial coverage and oceanographic resolution.

3.4.4 Description of salinity dynamics

Figure 23 shows the spatio-temporal collocations of the Baltic+ L3 and L4 SSS products and reanalysis with in situ measurements. It must be pointed out that the sampling frequency is too low to capture some relevant events in some in situ stations, as for example in the regions of the Bothnian Sea and the Gulf of Riga. An overall agreement in the main events is observed
490 between satellite, model and in situ along the time-series. However, salinity from reanalysis shows a very stable behaviour along the time-series for some particular regions, while the variability shown by the satellite SSS better reflects the variability captured by the in situ measurements. This is observed very clearly in the Northern Baltic Proper, in the Eastern and Western Gotland basin and in the Gulf of Riga.

Baltic+ SSS products can be very useful to validate the models in areas, where in situ data are sparse. Also, the location of the
495 salinity gradients and their variability is a valuable knowledge in evaluating the model performance. For example, Westerlund et al. (2018) discussed that model development is needed to better capture the large salinity gradients in the Gulf of Finland, but this work is hindered by the low temporal coverage of the data and lack of measurements from the eastern part of the Gulf of Finland. Same is also true for other sub-basins of the Baltic Sea and, especially, for the northern parts (Bothnian Sea and Bothnian Bay), where monitoring data is still too sparse. Thus, the new products will foster model development and provide
500 the possibility to assimilate SSS fields derived from space assets.

4 Conclusions

In this work, we present the first regional satellite-derived SSS maps over the Baltic Sea. To date, these are the unique dedicated remote sensed SSS products available over the region, mainly due to the technical difficulties for retrieving SSS from satellite measurements over this basin. Several technical improvements have been required, being the major ones (i) the study of the
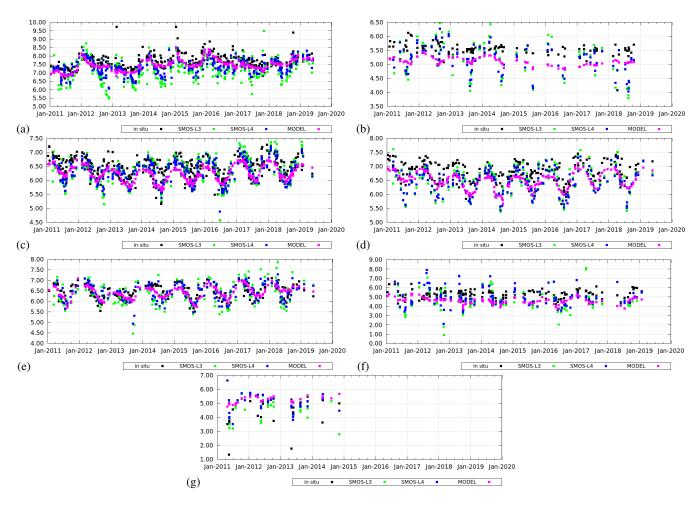
Figure 23. Spatio-temporal collocations of Baltic+ L3 SSS, Baltic+ L4 SSS, CMEMS Baltic reanalysis salinity fields with in situ salinity. Regions: (a) Bornholm Basin (BB), (b) Bothnian Sea (BS), (c) Northern Baltic Proper (NBP), (d) Eastern Gotland Basin (EGB), (e) Western Gotland Basin (WGB), (f) Gulf of Finland (GOF) and (g) Gulf of Riga (GOR).

505   dielectric constant models for the low temperatures and low salinity regimes of the Baltic Sea, and (ii) the characterization of SMOS SSS systematic errors depending also on the SST. These improvements developed in the context of the Baltic+ Salinity Dynamics project have a clear impact on other regional initiatives (such as EO4SIBS (4000127237/19/I-EF) and SO-Fresh (4000134536) projects) and in the SSS retrieval from satellite L-band measurements in general.

Baltic+ SSS products are proved to have a good spatio-temporal coverage with an accuracy of 0.7-0.8 psu for the L3 product
510   (9-day, $0.25°$) and around 0.4 psu in the case of the L4 product (daily, $0.05°$). Regions with higher errors and limited coverage are located in Arkona and Bornholm basins and Gulfs of Finland and Riga (section 3). The impact assessment of Baltic+ SSS products reveals that they provide valuable information about the changes in the salinity gradients and about the temporal

variability in the sea surface salinity. They also show a geophysically-consistent seasonal variability in surface salinity, which results from the melting of sea ice in spring and increased run-off from land when snow cover melts after the winter.

515   For all the above, Baltic+ SSS products can help in understanding the salinity dynamics of the basin. On one hand, this EO SSS data can fill the temporal and spatial observational gaps in the region left by the very sparse in situ measurements. On the other hand, Baltic+ SSS products can also be useful for the validation and improvement of numerical models. Besides, the capability of the Baltic+ SSS product to map the hoizontal gradients and their variability is of much value to evaluate the performance of models, and provide the possibility to assimilate SSS fields.

520   Several scientific studies with Baltic+ SSS data are currently in progress, such as (i) the analysis of the consistency between the structures detected in the Baltic+ SSS products with the ones detected in the SST and in the DOT (Dynamic Ocean Topography); and (ii) the use of Baltic+ SSS time-series as part of the HELCOM indicators to study the correlation between the SSS variability and the extreme events of different species in the Baltic Sea. Interactions with the scientific communities working in the Baltic, and in particular with Baltic Earth Working Group on Salinity Dynamics, has allowed to identify that

525   Baltic+ SSS products can help in some knowledge gaps (Lehmann et al., 2021), such as (i) the determination of the SSS annual trends in the basin in the last decade, and (ii) the study of the inflow and outflow dynamics at the entrance of the North Sea. For these potential applications, some additional technical developments in the product would be appropriated, mainly focused in applying a temporal correction of SSS maps without using external references, and applying fusion techniques at brightness temperature level for improving their quality in terms of coverage and spatial scales.

5   Data availability

530

Access to the data is provided by the Barcelona Expert Center, through its FTP service, for more details go to http://bec.icm.csic.es/ bec-ftp-service/. The L3 product is available per year in the directory becftpdata/OCEAN/SSS/SMOS/Baltic/v1.0/L3/9days. The DOI of the L3 product is: https://doi.org/10.20350/digitalCSIC/13859 (González-Gambau et al., 2021a). The L4 product is available per year in the directory becftpdata/OCEAN/SSS/SMOS/Baltic/v1.0/L4/daily. The DOI of the L4 product is: https:

535   //doi.org/10.20350/digitalCSIC/13860 (González-Gambau et al., 2021b). Seasonal averaged L4 SSS products are also available at HELCOM catalogue (https://metadata.helcom.fi/geonetwork/srv/eng/catalog.search#/metadata/9d979033-1136-4dd1-a09b-7ee9e512ad14) and they can be visualized in the HELCOM Map and Data service (https://maps.helcom.fi/website/mapservice/?datasetID= 9d979033-1136-4dd1-a09b-7ee9e512ad14).

545 been the responsibles of the management of the project. Diego Fernandez and Roberto Sabia have been the ESA project officers. All authors have reviewed the manuscript.

Competing interests. The authors declare that they have no conflict of interest.

Open Access Earth System Science Data Discussions

References

Axell, L.: Product User Manual of Baltic Sea Physical Reanalysis Product BALTICSEA_REANALYSIS_PHY_003_011, issue 2.0, Tech. rep., Copernicus Marine Environment Monitoring Service, https://catalogue.marine.copernicus.eu/documents/PUM/CMEMS-BAL-PUM-003-011.pdf, 2019.

565 Baltic+ team: Baltic+ Salinity Dynamics Requirements Baseline Document, ARG-003-054, v1r7, Tech. rep., ARGANS, BEC, FMI, 2019.

Boutin, J., Vergely, J. L., Marchand, S., D'Amico, F., Hasson, A., Kolodziejczyk, N., Reul, N., Reverdin, G., and Vialard, J.: New SMOS Sea Surface Salinity with reduced systematic errors and improved variability, Remote Sensing of Environment, 214, 115–134, https://doi.org/https://doi.org/10.1016/j.rse.2018.05.022, 2018.

Boutin, J., Vergely, J.-L., and Koehler, J.and Rouffi, F. R. N.: ESA Sea Surface Salinity Climate Change Initiative

570 (Sea_Surface_Salinity_CCI): Version 1.8 data collection., Tech. rep., https://doi.org/doi:10.5285/9ef0ebf847564c2eabe62cac4899ec41., 2019.

Boutin, J., Vergely, J. L., and Khvorostyanov, D.: SMOS SSS L3 maps generated by CATDS CEC LOCEAN. debias V5.0. SEANOE., Tech. rep., https://doi.org/https://doi.org/10.17882/52804#79565, 2020.

Canada Meteorological Center: CMC 0.2 deg global sea surface temperature analysis. Ver. 2.0., Tech. rep., PO.DAAC, CA, USA,

575 https://doi.org/https://doi.org/10.5067/GHCMC-4FM02, 2012.

Corbella, I., Torres, F., Duffo, N., Gonzalez, V., Camps, A., and Vall-llossera, M.: Fast Processing Tool for SMOS Data, in: IGARSS 2008 - 2008 IEEE International Geoscience and Remote Sensing Symposium, vol. 2, pp. II–1152–II–1155, https://doi.org/10.1109/IGARSS.2008.4779204, 2008.

Corbella, I., Torres, F., Camps, A., Duffo, N., and Vall-llossera, M.: Brightness-Temperature Retrieval Methods in Synthetic Aperture Ra-

580 diometers, IEEE Transactions on Geoscience and Remote Sensing, 47, 285–294, https://doi.org/10.1109/TGRS.2008.2002911, 2009.

Corbella, I., Durán, I., Wu, L., Torres, F., Duffo, N., Khazâal, A., and Martín-Neira, M.: Impact of Correlator Efficiency Errors on SMOS Land–Sea Contamination, IEEE Geoscience and Remote Sensing Letters, 12, 1813–1817, https://doi.org/10.1109/LGRS.2015.2428653, 2015.

Corbella, I., González-Gambau, V., Torres, F., Duffo, N., Durán, I., and Martín-Neira, M.: The MIRAS "ALL-LICEF"

585 calibration mode, in: 2016 IEEE International Geoscience and Remote Sensing Symposium (IGARSS), pp. 2013–2016, https://doi.org/10.1109/IGARSS.2016.7729519, 2016.

Corbella, I., Torres, F., Duffo, N., Durán, I., González-Gambau, V., and Martín-Neira, M.: Wide Field of View Microwave Interferometric Radiometer Imaging, Remote Sensing, 11, https://doi.org/10.3390/rs11060682, 2019.

Donlon, C. J., Martin, M., Stark, J., Roberts-Jones, J., Fiedler, E., and Wimmer, W.: The Operational Sea Surface Temperature and Sea

590 Ice Analysis (OSTIA) system, Remote Sensing of Environment, 116, 140–158, https://doi.org/https://doi.org/10.1016/j.rse.2010.10.017, https://www.sciencedirect.com/science/article/pii/S0034425711002197, Advanced Along Track Scanning Radiometer(AATSR) Special Issue, 2012.

Fischer, H. and Matthäus, W.: The importance of the Drogden Sill in the Sound for Major Baltic Inflows, Journal of Marine Systems, 9, 137–157, https://doi.org/https://doi.org/10.1016/S0924-7963(96)00046-2, https://www.sciencedirect.com/science/article/pii/S0924796396000462, 1996.

595 Fore, A., Yueh, S., Tang, W., Stiles, B., and Hayashi, A.: Combined Active/Passive Retrievals of Ocean Vector Wind and Sea Surface Salinity With SMAP, IEEE Transactions on Geoscience and Remote Sensing, 54, 7396–7404, https://doi.org/10.1109/TGRS.2016.2601486, 2016.

González-Gambau, V., Turiel, A., Olmedo, E., Martínez, J., Corbella, I., and Camps, A.: Nodal Sampling: A New Image Reconstruction Algorithm for SMOS, IEEE Transactions on Geoscience and Remote Sensing, 54, 2314–2328, https://doi.org/10.1109/TGRS.2015.2499324, 2015.

González-Gambau, V., Olmedo, E., Turiel, A., Martínez, J., Ballabrera-Poy, J., Portabella, M., and Piles, M.: Enhancing SMOS brightness temperatures over the ocean using the nodal sampling image reconstruction technique, Remote Sensing of Environment, 180, 205 – 220, https://doi.org/http://dx.doi.org/10.1016/j.rse.2015.12.032, http://www.sciencedirect.com/science/article/pii/S0034425715302534, special Issue: ESA's Soil Moisture and Ocean Salinity Mission - Achievements and Applications, 2016.

González-Gambau, V., Olmedo, E., González-Haro, C., García-Espriu, A., and Turiel, A.: Baltic Sea Surface Salinity L3 maps, https://doi.org/10.20350/digitalCSIC/13859, 2021a.

González-Gambau, V., Olmedo, E., González-Haro, C., García-Espriu, A., and Turiel, A.: Baltic Sea Surface Salinity L4 maps, https://doi.org/10.20350/digitalCSIC/13860, 2021b.

González-Gambau, V., Olmedo, E., Martínez, J., Turiel, A., and Durán, I.: Improvements on Calibration and Image Reconstruction of SMOS for Salinity Retrievals in Coastal Regions, IEEE Journal of Selected Topics in Applied Earth Observations and Remote Sensing, 10, 3064–3078, https://doi.org/10.1109/JSTARS.2017.2685690, 2017.

González-Gambau, V., Turiel, A., González-Haro, C., Martínez, J., Olmedo, E., Oliva, R., and Martín-Neira, M.: Triple Collocation Analysis for Two Error-Correlated Datasets: Application to L-Band Brightness Temperatures over Land, Remote Sensing, 12, https://doi.org/10.3390/rs12203381, https://www.mdpi.com/2072-4292/12/20/3381, 2020.

Hordoir, R., Axell, L., Höglund, A., Dieterich, C., Fransner, F., Gröger, M., Liu, Y., Pemberton, P., Schimanke, S., Andersson, H., Ljungemyr, P., Nygren, P., Falahat, S., Nord, A., Jönsson, A., Lake, I., Döös, K., Hieronymus, M., Dietze, H., Löptien, U., Kuznetsov, I., Westerlund, A., Tuomi, L., and Haapala, J.: Nemo-Nordic 1.0: a NEMO-based ocean model for the Baltic and North seas – research and operational applications, Geoscientific Model Development, 12, 363–386, https://doi.org/10.5194/gmd-12-363-2019, https://gmd.copernicus.org/articles/12/363/2019/, 2019.

JPL Climate Oceans and Solid Earth group: JPL SMAP Level 3 CAP Sea Surface Salinity Standard Mapped Image 8-Day Running Mean V4.2 Validated Dataset. Ver. 4.2., Tech. rep., Physical Oceanography Distributed Active Archive Center, CA, USA, https://doi.org/https://doi.org/10.5067/SMP42-3TPCS, 2019.

Klein, L. and Swift, C.: An improved model for the dielectric constant of sea water at microwave frequencies, IEEE Journal of Oceanic Engineering, 2, 104–111, https://doi.org/10.1109/JOE.1977.1145319, 1977.

Lehmann, A., Hinrichsen, H.-H., Getzlaff, K., and Myrberg, K.: Quantifying the heterogeneity of hypoxic and anoxic areas in the Baltic Sea by a simplified coupled hydrodynamic-oxygen consumption model approach, Journal of Marine Systems, 134, 20–28, https://doi.org/https://doi.org/10.1016/j.jmarsys.2014.02.012, https://www.sciencedirect.com/science/article/pii/S0924796314000414, 2014.

Lehmann, A., Myrberg, K., Post, P., Chubarenko, I., Dailidiene, I., Hinrichsen, H.-H., Hüssy, K., Liblik, T., Lips, U., Meier, H. E. M., and Bukanova, T.: Salinity dynamics of the Baltic Sea, Earth System Dynamics Discussions, 2021, 1–36, https://doi.org/10.5194/esd-2021-15, https://esd.copernicus.org/preprints/esd-2021-15/, 2021.

Leppäranta, M. and Myrberg, K.: The Physical Oceanography of the Baltic Sea, Springer-Verlag, Berlin-Heidelberg, New York., 2009.

Martín-Neira, M., Oliva, R., Corbella, I., Torres, F., Duffo, N., Durán, I., Kainulainen, J., Closa, J., Zurita, A., Cabot, F., Khazaal, A., Anterrieu, E., Barbosa, J., Lopes, G., Tenerelli, J., Díez-García, R., Fauste, J., Martín-Porqueras, F., González-Gambau, V., Turiel, A., Delwart, S., Crapolicchio, R., and Suess, M.: SMOS instrument performance and calibration after six years in orbit, Remote Sensing of

Environment, 180, 19 – 39, https://doi.org/http://dx.doi.org/10.1016/j.rse.2016.02.036, http://www.sciencedirect.com/science/article/pii/S0034425716300645, special Issue: ESA's Soil Moisture and Ocean Salinity Mission - Achievements and Applications, 2016.

Matthäus, W. and Franck, H.: Characteristics of major Baltic inflows—a statistical analysis, Continental Shelf Research, 12, 1375–1400, https://doi.org/https://doi.org/10.1016/0278-4343(92)90060-W, https://www.sciencedirect.com/science/article/pii/027843439290060W, 1992.

640

Meier, H. E. M., Kjellström, E., and Graham, L. P.: Estimating uncertainties of projected Baltic Sea salinity in the late 21st century, Geophysical Research Letters, 33, https://doi.org/https://doi.org/10.1029/2006GL026488, https://agupubs.onlinelibrary.wiley.com/doi/abs/10.1029/2006GL026488, 2006.

Meissner, T. and Wentz, F. J.: The complex dielectric constant of pure and sea water from microwave satellite observations, IEEE Transactions on Geoscience and Remote Sensing, 42, 1836–1849, https://doi.org/10.1109/TGRS.2004.831888, 2004.

645

Meissner, T., Wentz, F. J., and Manaster, A.: Remote Sensing Systems SMAP Ocean Surface Salinities [Level 2C, Level 3 Running 8-day, Level 3 Monthly], Version 3.0 validated release, Tech. rep., Remote Sensing Systems, Santa Rosa, CA, USA. , https://doi.org/10.5067/SSSSS-TTTTT, http://www.remss.com/missions/smap, available online at www.remss.com/missions/smap, 2018.

Merchant, C. J., Embury, O., Bulgin, C. E., Block, T., Corlett, G. K., Fiedler, E., Good, S. A., Mittaz, J., Rayner, N. A., Berry, D., et al.: Satellite-based time-series of sea-surface temperature since 1981 for climate applications, Scientific data, 6, 1–18, 2019.

650

Oliva, R., Daganzo, E., Richaume, P., Kerr, Y., Cabot, F., Soldo, Y., Anterrieu, E., Reul, N., Gutierrez, A., Barbosa, J., and Lopes, G.: Status of Radio Frequency Interference (RFI) in the 1400–1427 MHz passive band based on six years of SMOS mission, Remote Sensing of Environment, 180, 64 – 75, https://doi.org/https://doi.org/10.1016/j.rse.2016.01.013, http://www.sciencedirect.com/science/article/pii/S0034425716300141, special Issue: ESA's Soil Moisture and Ocean Salinity Mission - Achievements and Applications, 2016.

655

Olmedo, E., Martínez, J., Umbert, M., Hoareau, N., Portabella, M., Ballabrera-Poy, J., and Turiel, A.: Improving time and space resolution of SMOS salinity maps using multifractal fusion, Remote Sensing of Environment, 180, 246 – 263, https://doi.org/https://doi.org/10.1016/j.rse.2016.02.038, http://www.sciencedirect.com/science/article/pii/S0034425716300669, special Issue: ESA's Soil Moisture and Ocean Salinity Mission - Achievements and Applications, 2016.

Olmedo, E., Martínez, J., Turiel, A., Ballabrera-Poy, J., and Portabella, M.: Debiased non-Bayesian retrieval: A novel approach to SMOS Sea Surface Salinity, Remote Sensing of Environment, 193, 103 – 126, https://doi.org/https://doi.org/10.1016/j.rse.2017.02.023, http://www.sciencedirect.com/science/article/pii/S0034425717300822, 2017.

660

Olmedo, E., Gabarró, C., González-Gambau, V., Martínez, J., Ballabrera-Poy, J., Turiel, A., Portabella, M., Fournier, S., and Lee, T.: Seven Years of SMOS Sea Surface Salinity at High Latitudes: Variability in Arctic and Sub-Arctic Regions, Remote Sensing, 10, https://doi.org/10.3390/rs10111772, https://www.mdpi.com/2072-4292/10/11/1772, 2018a.

665

Olmedo, E., Taupier-Letage, I., Turiel, A., and Alvera-Azcárate, A.: Improving SMOS Sea Surface Salinity in the Western Mediterranean Sea through Multivariate and Multifractal Analysis, Remote Sensing, 10, https://doi.org/10.3390/rs10030485, https://www.mdpi.com/2072-4292/10/3/485, 2018b.

Olmedo, E., González-Gambau, V., Turiel, A., Guimbard, S., González-Haro, C., Martínez, J., Gabarró, C., Portabella, M., Arias, M., Sabia, R., Oliva, R., and Corbella, I.: Towards an enhanced SMOS Level-2 Ocean Salinity product, IEEE Journal of Selected Topics in Applied Earth Observations and Remote Sensing, 13, 6434–6453, 2020.

670

Olmedo, E., González-Gambau, V., Turiel, A., González-Haro, C., García-Espriu, A., Gregoire, M., Álvera-Azcárate, A., Buga, L., and Rio, M.-H.: New SMOS SSS maps in the framework of the Earth Observation data For Science and Innovation in the Black Sea, Earth System Science Data Discussions, pp. 1–40, 2021a.

Olmedo, E., González-Haro, C., Hoareau, N., Umbert, M., González-Gambau, V., Martínez, J., Gabarró, C., and Turiel, A.: Nine
675   years of SMOS sea surface salinity global maps at the Barcelona Expert Center, Earth System Science Data, 13, 857–888,
       https://doi.org/10.5194/essd-13-857-2021, https://essd.copernicus.org/articles/13/857/2021/, 2021b.

Omstedt, A., Elken, J., Lehmann, A., Leppäranta, M., Meier, H., Myrberg, K., and Rutgersson, A.: Progress in
       physical oceanography of the Baltic Sea during the 2003–2014 period, Progress in Oceanography, 128, 139–171,
       https://doi.org/https://doi.org/10.1016/j.pocean.2014.08.010,   https://www.sciencedirect.com/science/article/pii/S0079661114001335,
680   2014.

Remote Sensing Systems: MWIR optimum interpolated SST data set. Ver. 5.0., Tech. rep., PO.DAAC, CA, USA,
       https://doi.org/https://doi.org/10.5067/GHMWI-4FR05, 2017.

Remote Sensing Systems (RSS): SMAP Sea Surface Salinity Products. Ver. 4.0, Tech. rep., Physical Oceanography Distributed Active
       Archive Center, CA, USA, https://doi.org/https://doi.org/10.5067/SMP40-2SOCS, 2019.

685   Sabater, J. and De Rosnay, P.: Milestone 2 Tech Note - Parts 1/2/3: Operational Pre-processing chain, Collocation software devel-
       opment and Offline monitoring suite, Tech. rep., ECMWF, http://www.ecmwf.int/en/elibrary/11316-milestone-2-tech-note-parts-1/2/
       3-operational-pre-processing-chain-collocation, 2010.

SeaDataNet Baltic Climatology: Baltic Sea - Temperature and Salinity Climatology V1.1., Tech. rep., Institute of Marine Research, Alfred-
       Wegener-Institute for Polar- and Marine Research, Institute of Meteorology and Water Management National Research Institute, Maritime
690   Branch in Gdynia (IMWM MB), Institute of Oceanology, Polish Academy of Sciences (IO PAS), Environmental Protection Agency
       (EPA), National Oceanography Centre, Liverpool, GEOMAR Helmholtz Centre for Ocean Research Kiel, Shom, Swedish Meteorological
       and Hydrological Institute, Stockholm Marine Research Centre, SMF, Umea Marine Sciences Centre, UMF, Finnish Institute of Marine
       Research (FIMR), NIOZ Royal Netherlands Institute for Sea Research, Department of Marine Research of the Environmental Protection
       Agency, P.P.Shirshov Institute of Oceanology, RAS, Marine Systems Institute at Tallinn University of Technology, Aarhus University,
695   Department of Bioscience, Marine Ecology Roskilde, Russian State Hydrometeorological University, St-Petersburg, Odessa Branch of
       SOI (State Oceanographic Institute), https://doi.org/10.12770/bf35a7c5-c843-4a23-8040-07ddcf3d8e71.

Turiel, A., Isern-Fontanet, J., and Umbert, M.: Sensibility to noise of new multifractal fusion methods for ocean variables, Nonlinear pro-
       cesses in geophysics, 21, 291 – 301, https://doi.org/https://doi.org/10.5194/npg-21-291-2014, 2014.

Umbert, M., Hoareau, N., Turiel, A., and Ballabrera-Poy, J.: New blending algorithm to synergize ocean variables: The case of SMOS
700   Sea Surface Salinity maps, Remote Sensing of Environment, 146, 172 – 187, https://doi.org/https://doi.org/10.1016/j.rse.2013.09.018,
       http://www.sciencedirect.com/science/article/pii/S0034425713003556, liege Colloquium Special Issue: Remote sensing of ocean colour,
       temperature and salinity, 2014.

Westerlund, A., Tuomi, L., Alenius, P., Miettunen, E., and Vankevich, R. E.: Attributing mean circulation patterns to physical phenomena
       in the Gulf of Finland, Oceanologia, 60, 16–31, https://doi.org/https://doi.org/10.1016/j.oceano.2017.05.003, https://www.sciencedirect.
705   com/science/article/pii/S0078323417300623, 2018.

Yueh, S., West, R., Wilson, W., Li, F., Njoku, E., and Rahmat-Samii, Y.: Error sources and feasibility for microwave remote sensing of ocean
       surface salinity, IEEE Transactions on Geoscience and Remote Sensing, 39, 1049–1060, https://doi.org/10.1109/36.921423, 2001.

Zhou, Y., Lang, R. H., Dinnat, E. P., and Vine, D. M. L.: L-Band Model Function of the Dielectric Constant of Seawater, IEEE Transactions
       on Geoscience and Remote Sensing, 55, 6964–6974, https://doi.org/10.1109/TGRS.2017.2737419, 2017.

710   Zine, S., Boutin, J., Font, J., Reul, N., Waldteufel, P., Gabarró, C., Tenerelli, J., Petitcolin, F., Vergely, J., Talone, M., and Delwart, S.:
        Overview of the SMOS Sea Surface Salinity Prototype Processor, IEEE Transactions on Geoscience and Remote Sensing, 46, 621–645,
        https://doi.org/10.1109/TGRS.2008.915543, 2008.